Computational investigation of Au···H hydrogen bonds involving neutral Au^{I} *N*-heterocyclic carbene complexes and amphiprotic binary hydrides

Ferdinand Groenewald, Helgard G. Raubenheimer, Jan Dillen and Catharine Esterhuysen*

Department of Chemistry and Polymer Science, Stellenbosch University, Private Bag X1, Matieland, Stellenbosch, 7602, South Africa.

*Correspondence author, ce@sun.ac.za, Tel: +27 21 808 3345.

ORC-IDs: FG: 0000-0002-8893-3838; JD: 0000-0002-9664-2395; CE: 0000-0002-0135-2118.

Abstract

In this computational study we investigate the ability of various neutral R-Au^{I}-NHC (NHC = *N*-heterocyclic carbene) complexes [R = H, CH_3, Cl, OH] to form hydrogen bonds with the amphiprotic binary hydrides NH_3, H_2O and HF. Optimised geometries of the adducts calculated at various levels of theory all exhibit Au···HX hydrogen bonds. In adducts of complexes containing NHC ligands with α-N–H units $(NH)_{carbene}$···XH interactions also exist, yielding hydrogen-bonded rings with graph-set notation $R_2^2(6)$ that correspond to pseudo chelates with κ^2C,H coordination. AIM analysis at the MP2/aug-cc-pVTZ-pp level of theory indicates that the $(NH)_{carbene}$···XH hydrogen bonds are generally stronger than the Au···HX interactions, except for those involving HF. The Au···HX interactions vary with the Lewis basicity of the Au(I) centre as a result of the nature of the R ligand, while the $(NH)_{carbene}$···XH hydrogen bonds are unaffected by R. Energy Decomposition Analysis at the BP86/TZP level of theory identifies the origin of this difference as the greater component of polarisation involved in Au···HX interactions. Replacing the α(N)Hs with methyl groups prevents formation of a strong $(NH)_{carbene}$···XH interaction, thus reducing the overall stabilisation of the adducts. Nevertheless, the Au···H interactions remain largely unchanged and are strong enough to sustain the hydrogen-bonded complexes, although weak C–H···X interactions are often also present.

Keywords

Gold(I) complexes; N-heterocyclic carbenes; hydrogen bonds; polarisation.

Acknowledgements

The Rhasatsha High Performance Computer Center at Stellenbosch University and the Centre for High Performance Computing in Cape Town are thanked for computational resources. The National Research Foundation (JD: CSUR grant no. 91553; CE: CPRR grant no. 113331) and the University of Stellenbosch are thanked for financial support. Opinions expressed and conclusions arrived at are those of the authors and are not necessarily to be attributed to the NRF.

Introduction

In 1993, Kazarian and coworkers [1] posed the question "Is Intermolecular Hydrogen-Bonding to Uncharged Metal Centres of Organometallic Compounds Widespread in Solution?" and considered the examples of Co, Rh and Ir. They pointed out that the protonation of a metal centre is of importance, since it is widely recognised as a key step in organometallic chemistry, but is somewhat poorly understood even though hydrogen bonding to the group 9 metals can be observed by IR and is quite widespread. We have recently shown [2,3] that the Au(I) centre can act as a hydrogen-bond (H-bond) acceptor when it is coordinated to two strongly electron-donating ligands. The ligands induce a partial negative charge on the gold atom, enabling the Au(I) centre to act as a Lewis base and thus as an H-bond acceptor to a wide variety of H-bond donors. Although the ligands were typically negatively charged, yielding anionic complexes, we were able to show that even neutral complexes could form weak hydrogen bonds with H_2O [2].

Nevertheless, there is little experimental data available for $Au^I\cdots H$ interactions [4]. This could be due to the presence of complementary interactions that stabilise the geometries of the $Au\cdots H$ interactions [2]. Two of the few examples of crystal structures exhibiting the $Au^I\cdots H$ interaction [5] are neutral complexes containing the *N*-methylbenzothiazole-2-thione (mbtt) ligand coordinated to the Au(I) centre, with the second ligand being either Cl^- or Br^-. Atoms in Molecules analysis of the crystal structures showed that the C-H$\cdots$Au contact was the strongest interaction, but that a second hydrogen bond involving the neighbouring CH group on the mbtt interacting with the coordinating thione atom was also present, thus forming a 6-membered pseudo-chelate ring. The presence of such multiple interactions may be indicative of cooperativity, which occurs when a species behaves as both a hydrogen bond donor and an acceptor, leading to additional stabilisation greater than the sum of the two hydrogen bonds [6].

Taking our lead from a study by Kryachko on hydrogen bonds involving Au^- [7], and the work of Brammer on electron-rich anionic transition-metal complexes forming hydrogen bonds [8], our previous reports [2,3] have focussed primarily on anionic complexes. However, anionic Au^I complexes are fairly uncommon, only 7.82% (485) of 6202 crystal structures containing Au^I compounds in the Cambridge Structural Database [9; August 2018 update] contain anionic Au^I species, as compared to 4062 neutral or 1655 cationic Au(I) species. Hence, it is of greater interest to determine the ability of neutral Au^I centres to act as hydrogen bond acceptors.

In particular, we aimed to investigate how important the presence of a second hydrogen-bonding interaction is for the stabilisation of $Au^I\cdots H$ hydrogen bonds. We have therefore

studied the interactions between a range of neutral RAu(NHC) (NHC = *N*-heterocyclic carbene) complexes with a series of amphiprotic main-group hydrides, namely NH_3, H_2O and HF. Our main objective was to determine if an Au···H interaction forms and what its nature is as defined by geometrical and AIM parameters. In addition, with the range of complexes chosen we aimed to determine how the R group influences the formation of the Au···H interaction and its properties. NHCs were selected as neutral ligands since they are electron donating, as required to enable the Au(I) centre to act as a hydrogen-bond acceptor. In addition, synthesis of Au(NHC)X (X = Cl, Br and I) complexes in a one-step methodology is typically "straightforward", as described by Collado *et al.* [10]. Furthermore, an (NHC)AuH complex has been synthesised by Phillips *et al*. [11], while Nahra *et al*. [12] have recently proposed a novel route to obtain (NHC)AuOH complexes in multi-gram scale. Gold complexes with unsubstituted NHCs are more difficult to synthesise, for instance it is not possible using Arduengo's method although an alternative route starting from imidazole has proven successful [13] and partially unsubstituted Au-NHCs have been prepared [14]. However, to investigate whether the formation of pseudo chelates is necessary to stabilise the Au···H interaction it was nevertheless decided to utilise simplified model Au^I complexes consisting of unsubstituted imidazolylidene, in combination with various anionic secondary ligands, as the first step in the study presented here. In addition to the anionic groups H^-, Cl^- and OH^-, CH_3^- was also included as a second ligand as we recently showed [2,3] that since the methyl ligand is a good electron donor the $[(Me)_2Au]^-$ complex forms strong unassisted H-bonds. The most stable hydrogen-bonded adducts of $[(Me)_2Au]^-$ with NH_3, OH_2 and FH involve interaction energies of -6.9 kcal/mol, -11.5 kcal/mol and-16.0 kcal/mol, respectively, as a result of the influence of the CH_3 ligand on the Au^I centre [3]. In addition, the linear geometries observed for these interactions suggest that they can be classified as moderately strong hydrogen bonds, which, according to Jeffrey [15], typically have E_{INT} values of 4-15 kcal/mol and angles of 130-180º. The role of the formation of pseudo chelates was investigated with respect to the abilities of both the NHC ligands and the amphiprotic hydrides to form hydrogen bonds. In the former case, the NHC ligands were varied with respect to the number of available N-H hydrogen bond donors, by utilising the model ligands imidazol-2-ylidene (NHC1) with two α-N–H units, pyrrol-2-ylidene (NHC2, one α-N–H unit) and 1,3-dimethylimidiazol-2-ylidene (NHC3, no N–H units).

Methods

Our investigation was performed using two Density Functional Theory (DFT) methods and the MP2 method combined with correlation consistent triple-zeta quality basis sets, which we have shown previously give good descriptions for interactions involving related complexes [2, 3, 16b]. In particular, the calculated interaction energies correspond to those determined at the CCSD(T)/aug-cc-pVTZ-pp level of theory [16b], and in previous studies [7, 16c]. MP2 is known to overestimate dispersion interactions, although our previous results [16], and those of others [17], have shown that MP2 combined with the smaller basis set cc-pVTZ provides a better E_{INT} value than the larger aug-cc-pVTZ basis set. The DFT methods were found to give similar results to those obtained with MP2, so for the large systems with NHC3 the B3LYP/aug-cc-pVTZ values are reported since MP2 is too computationally expensive.

All geometry optimisations were performed in the gas phase, with counterpoise corrections [18, 19], utilising the Gaussian 09 revD.01 [20] software package. During the optimisations no symmetry constraints were enforced and frequencies were calculated to verify that geometries were energy minima.

The counterpoise corrected interaction energy was calculated using:

$$E_{INT} = E_{AB}^{BSSE} - (E_A + E_B)$$

where the energies of fragments A and B (E_A and E_B) were calculated with the individual geometries extracted from the AB adduct.

The B3LYP [21-23] and TPSSTPSS (TPSS) [24] density functionals were utilised in combination with the aug-cc-pVTZ-pp [25] basis set describing the Au atom in combination with the effective core potential (ECP) developed by Figgen *et al*. [26]. The pseudopotential incorporated into this basis set describes the relativistic effects exhibited by Au, which we have previously shown is vital for accurate calculation of hydrogen bonds involving gold [2, 3]. The other atoms (H, C, F, O, N) were represented by the aug-cc-pVTZ [27, 28] basis set. The MP2 [29,30] method was employed in combination with the cc-pVTZ-pp and the aug-cc-pVTZ-pp basis sets [25] with the correct ECP [26] corresponding to the Au atom for each basis set. When the cc-pVTZ-pp or aug-cc-pVTZ-pp basis sets were employed to describe Au, the corresponding basis sets, cc-pVTZ and aug-cc-pVTZ, were utilised to describe the other atoms, to ensure all atoms are described by the same type of basis set. All basis sets were downloaded from the EMSL basis set exchange website [31, 32]. The ChemCraft [33] suite was utilised for visualisation of the output files.

The van der Waals (vdW) radii of N, O, F and Au were obtained from Bondi [34] and were selected as 1.55 Å, 1.52 Å, 1.47 Å and 1.66 Å, respectively. The vdW radius for the H-atom

was selected as 1.2 Å. The sum of vdW radii for Au···H, N···H, O···H and F···H are therefore 2.86 Å, 2.75 Å, 2.72 Å and 2.67 Å, respectively.

The wave function files (wfx) obtained from Gaussian at the MP2/aug-cc-pVTZ-pp level of theory were analysed with the Atoms In Molecules (AIM) analysis program AIMAll [35] version 14.06.21. The electron density [ρ_b ($e a_0^{-3}$)] and the Laplacian of the electron density $\nabla^2(\rho_b)$ ($e a_0^{-5}$) at the intermolecular Bond Critical Points (BCPs), were obtained as is from AIMAll. The *b* subscript indicates that it is a property at the intermolecular BCP of the H-bond. Values for the total electronic energy density, $H_b\ (au) = -K\ (au)$, were also determined, however, these are known to fluctuate when ECPs are utilised, as the electron density is not completely recovered and will not be discussed further [36, 37].

Noncovalent Interaction (NCI) plots developed by Johnson *et al*. [38] were also calculated from the wfx file and were graphically investigated and displayed utilising AIMAll. The Reduced Electron Density Gradient (RDG) isosurfaces were calculated with a resolution of 0.04 au. The isosurface visualisation of the RDG was calculated at a value of 0.5 au and with a minimum and maximum electron densities of 0.0001 and 0.05 $e a_0^{-3}$, respectively. The RDG surfaces were visualised by mapping sign(λ_2)ρ(**r**) onto them. The colour scale was chosen so that red indicates a negative (λ_2)ρ(**r**) value and blue a positive value of (λ_2)ρ(**r**), indicating attractive and repulsive interactions, respectively.

The Gaussian optimised geometries were used to perform Energy Decomposition Analysis (EDA) [39] based on the methods of Morokuma [40] and Ziegler and Rauk [41] with the 2017.113 release of the ADF software suite [42] at the BP86/TZP level of theory [43]. Core electrons were treated with a small core frozen core approach and scalar relativistic effects were included by applying the zeroth-order regular approximation (ZORA) [44]. In EDA the instantaneous interaction ΔE_{int} consists of four components, such that

$$\Delta E_{int} = \Delta E_{elstat} + \Delta E_{Pauli} + \Delta E_{orb} + \Delta E_{disp}$$

where ΔE_{elstat} and ΔE_{orb} are attractive electrostatic and orbital overlap terms and ΔE_{Pauli} indicates the repulsion between the two fragments as a result of two electrons with the same spin being forbidden to occupy the same region in space. The dispersion energy component, ΔE_{disp}, is determined using Grimme's DFT-D3-BJ dispersion correction [45].

Results and Discussion

NHC1 complexes

The four Au(NHC1)R complexes with the unsubstituted N-heterocyclic carbene NHC1 = imidazol-2-ylidene and R = H (**1**), H_3C (**2**), Cl (**3**), HO (**4**) can be divided into two groups, namely those with electron-donating R groups (complexes **1** and **2**), and those with electron-withdrawing groups (complexes **3** and **4**). The optimised geometries for the H-bonded adducts of NH_3, H_2O and HF with complexes **1** – **4** are shown in Figure 1. Within each adduct there are two hydrogen bonds, which together form a pseudo-chelate ring with graph set notation $R_2^2(6)$ [46]. The interaction energies and values for selected geometrical parameters, are shown in Figure 1, and are also given in Tables S1-S4 in the ESI. The hydrogen atoms in the interacting molecules appear to be pointing towards the R ligand (see Figure 1), suggesting that competing R···HX interactions may be present. These distances are given in Tables S1-S4 in the ESI for reference.

Geometrical parameters can be indicators of the strength of the H-bond, with shorter Au···H distances, longer H-X bonds and more linear Au···H-X angles generally correlating with stronger H-bonds to the metal, although care should be taken since the application of this estimation has limitations [47]. The Au···H distances remain relatively constant for complexes **1** and **2**, but longer for complexes **3** and **4**, with the same H-bond donor, while for each complex the distances increase HF < H_2O < NH_3. On this basis, the results suggest that the Au···HX hydrogen bonds decrease in strength HF > H_2O > NH_3, with the Au···H distances being about 80% of the sum of the van der Waals radii (sum vdW) for HF, 90% of sum vdW for H_2O and larger than sum vdW for NH_3, depending on the electron-withdrawing or -donating nature of the R ligand. The ligands show an influence on the Au···H distance, which suggests that the Au···H interaction strength decreases with the ligands in the order H^- ~ CH_3^- > OH^- > Cl^-. This is similar to our previous result [2] that electron-donating ligands provide electron density on the gold centre thus allowing it to behave as a Lewis base. The Au···H distances are comparable with the C-H···Au distances of 2.82 Å and 2.84 Å found by Koskinen *et al.* [5], but longer than the intramolecular N-H···Au hydrogen bonds identified by Berger *et al.* (2.06 Å) [48] and Rigoulet *et al.* (2.24 Å) [49] as part of six-membered pseudo-chelate rings. On the other hand, the Au···H-X angles deviate substantially from linearity with the smallest angle being 125.5º for **3.NH3**, and the largest angle being 154.8º for **2.HF**. This could be indicative of an interaction with the R group, but the R···HX distances (shown in Tables S1-S4 of the ESI) are considerably longer than the Au···HX distances, suggesting that such interactions would be negligible in comparison. This is in contrast with the anionic complex $HAuCH_3^-$,

which exhibits H···H interactions between the hydride R group and the HX hydrogen bond donors [2, 50]. In addition, even the relatively strong interactions calculated by Kryachko [7] and ourselves [2,3] for H_2O and NH_3 interacting with the benchmark hydrogen-bond acceptor, the auride anion, exhibited Au···HX angles of ~160°. In the current study where weaker interactions would be expected, owing to the Au complex being neutral, all the angles are below 160º. However, it should be noted that smaller Au···H-X angles correspond not only to a lengthening of the Au···H distance, but also to short $(NH)_{carbene}$···X distances, indicative of potential NH···X hydrogen bonds. The deviation from linearity can thus be explained as the H-bond donor orientating itself to maximise interactions with both the Au and carbene-NH group. The $(NH)_{carbene}$···X contact distances are short, with concomitantly longer N-H bond lengths, as would be expected for typical hydrogen bonds. Interestingly, the $(NH)_{carbene}$···X contact distances and carbene N–H bond lengths are independent of R, however the linearity of the $(N–H)_{carbene}$···X angle increases as the Au···H distance lengthens with changing R (Figure 1).

The interaction energies follow the opposite trend to that found above for the Au···H distances, with the strength decreasing: NH_3 > H_2O > HF. Therefore there is no correlation between Au···H lengths and E_{INT} values. Instead, closer inspection of the variation in $(NH)_{carbene}$···XH distances reveals that for each Au complex the E_{INT} value increases as the $(NH)_{carbene}$···X hydrogen bond length decreases. This is not unexpected, as these hydrogen bonds are anticipated to be of moderate strength [14], as opposed to the Au···HX interactions, which would be expected to be weaker since the neutral Au(I) centre is a poorer H-bond acceptor. Since there is a better correlation between the E_{INT} values and the geometrical parameters of the $(NH)_{carbene}$···X H-bond rather than those of the Au···HX interaction, we can postulate that the NH···XH interaction has a greater contribution to the total E_{INT} value than the Au^{I}···H interaction. Nevertheless, since the bond lengths of the $(NH)_{carbene}$···X hydrogen bonds are almost identical for a specific XH species the variation in E_{INT} values with changing R groups should be as a result of the variation in the strength of the Au···HX hydrogen bonds. However, no clear trends with regard to Au···H strengths are evident, which suggests that the energetic penalty of the deformation of the $(NH)_{carbene}$···X hydrogen bonds away from linearity also plays a role in the overall stabilisation of the system.

Since topological parameters such as the electron density and Laplacian of the electron density [51] can be useful to determine if an interaction is a hydrogen bond [52-54], Atoms in Molecules (AIM) analysis was performed in conjunction with NCI plots (see Table 3 and selected plots in Figure 2 with the remainder in Figure S1 in the ESI).

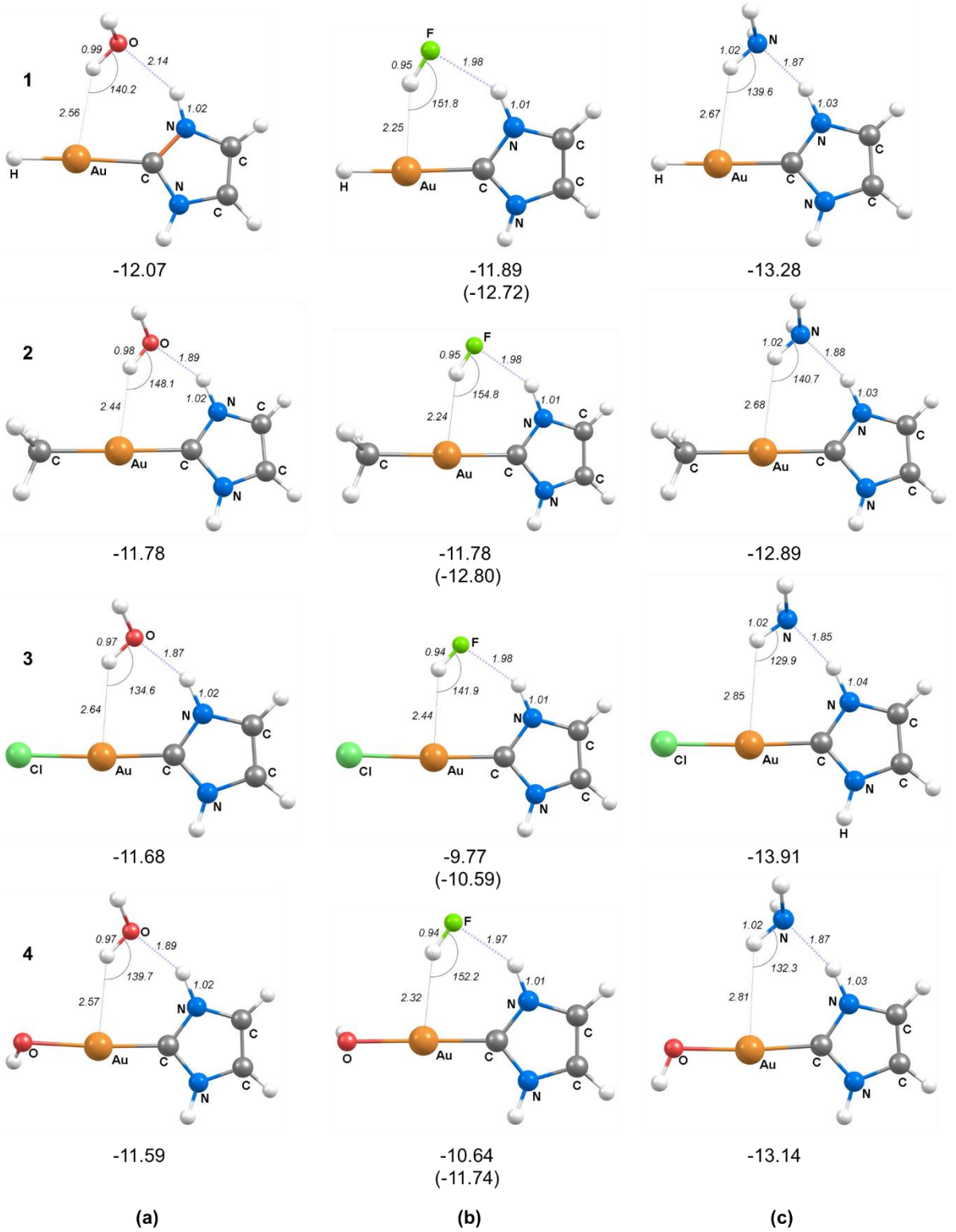

Figure 1 – Optimised geometries of complexes **1** – **4** H-bonded to (a) NH_3, (b) H_2O and (c) HF at the MP2/aug-cc-pVTZ-pp level of theory. Distances and angles are in Å and degrees, respectively. Counterpoise-corrected values for the interaction energies in kcal/mol, E_{INT}, at the MP2/aug-cc-pVTZ-pp level of theory are given below each adduct (E_{INT} values at the B3LYP-D3/aug-cc-pVTZ-pp level of theory are given in parenthesis).

The most important characteristics of the molecular graphs in Figure 2 are the atomic interaction lines, with associated bond critical points (BCPs) present for the Au···H and $(NH)_{carbene}$···XH interactions in all H-bonded adducts. These are indicative of overlap between atoms and can be interpreted as confirmation that noncovalent interactions exist. The lack of atomic interaction lines between the hydrogen bond donors and the R groups confirms our earlier assumption that the H···R distances are too long for such an interaction to be present. The NCI plots (Figure 2), which supplement the AIM analysis by highlighting weak interactions (both attractive and repulsive), also show no evidence of RDG surfaces corresponding to weak interactions involving the R ligand.

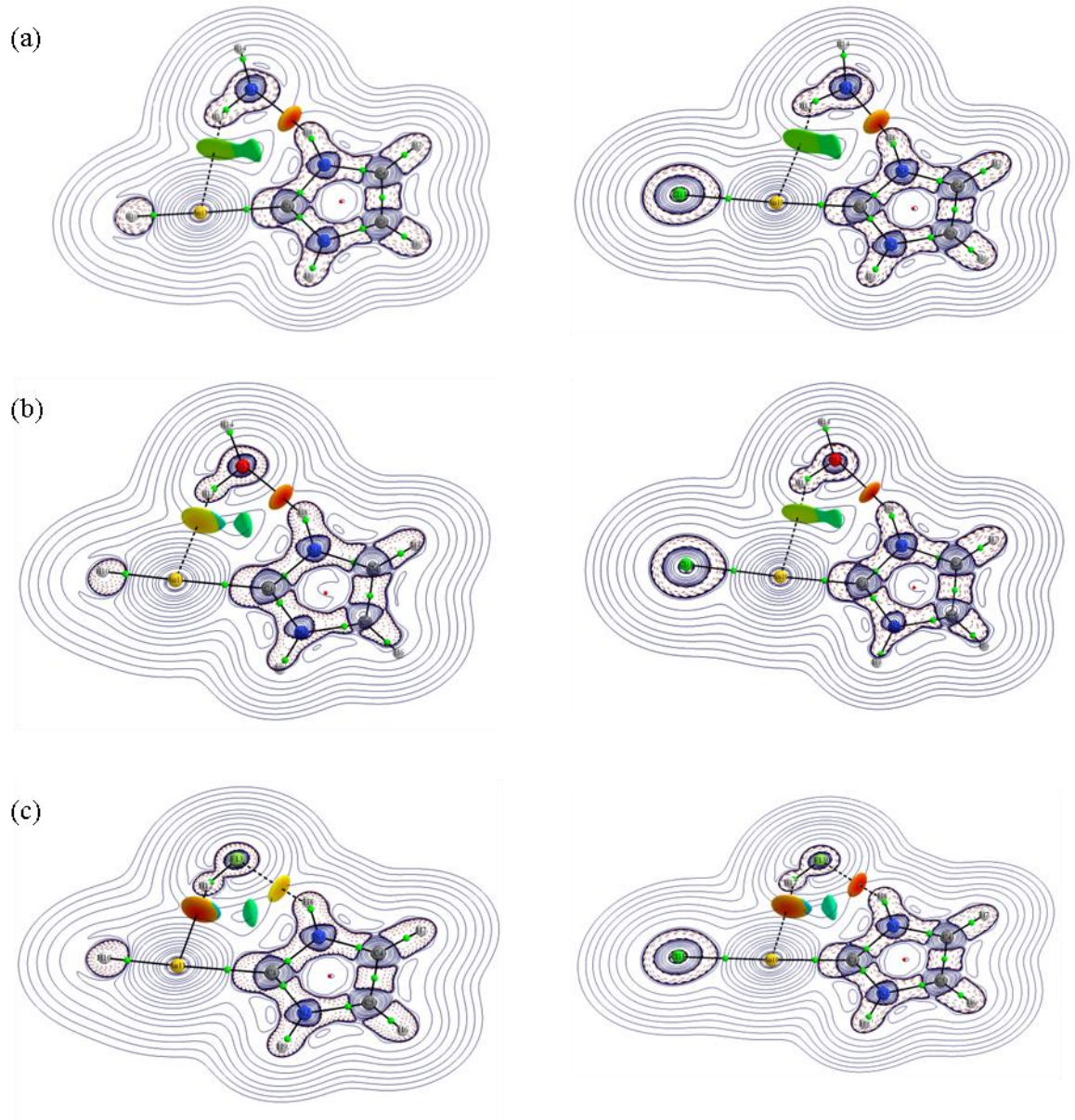

Figure 2 – The two-dimensional contour plot of $\nabla^2(\rho_b)$ (ea_0^{-5}) with the NCI plots shown as green to red areas on the images for complexes **1** (left) and **3** (right) with (a) NH_3, (b) H_2O and (c) HF.

The colouring of the NCI plots shown in Figure 2 is based on a scale relative to the largest $(\lambda_2)\rho(\mathbf{r})$ value for each respective adduct. In terms of repulsion and attraction cyan and blue regions represent nonbonding or repulsive interactions whereas the red, yellow and lime green regions indicate stabilising interactions. The lime green regions indicate $(\lambda_2)\rho(\mathbf{r})$ values of weaker H-bonds, typically dispersion-type interactions, whereas red regions indicate strong interactions. Most importantly, the NCI plots contrast the two H-bonds, confirming that in general the NH···XH interaction is more stabilising than the Au^I···H interaction, except for interactions involving HF. In these cases the Au^I···H interactions contribute greater stabilisation to E_{INT} than the NH···XH hydrogen bonds. In addition, the NCI plots show that there is no detectable stabilisation between the H-bond donor and the formally anionic ligand coordinated to Au(I), while there seems to be a nonbonding/repulsive interaction between the heteroatom of the H-bond donor and the NHC carbon atom coordinated to Au(I).

Table 1 – Selected AIM parameters at the bond critical points for the indicated hydrogen bonds in the optimised structures of complexes **1** – **4** H-bonded to NH_3, H_2O and HF at the MP2/aug-cc-pVTZ-pp level of theory.

		Au···H-X		**$(NH)_{carbene}$···X-H**	
		$\boldsymbol{\rho_b}$ $(\boldsymbol{e a_0^{-3}})$	$\boldsymbol{\nabla^2(\rho_b)}$ $(\boldsymbol{e a_0^{-5}})$	$\boldsymbol{\rho_b}$ $(\boldsymbol{e a_0^{-3}})$	$\boldsymbol{\nabla^2(\rho_b)}$ $(\boldsymbol{e a_0^{-5}})$
1	NH_3	0.012	0.036	0.036	0.086
	H_2O	0.018	0.049	0.028	0.104
	HF	0.026	0.055	0.019	0.090
2	NH_3	0.012	0.035	0.035	0.085
	H_2O	0.018	0.049	0.027	0.104
	HF	0.027	0.054	0.019	0.091
3	NH_3	0.008	0.027	0.038	0.084
	H_2O	0.012	0.037	0.029	0.105
	HF	0.017	0.047	0.019	0.090
4	NH_3	0.009	0.029	0.036	0.084
	H_2O	0.014	0.041	0.028	0.103
	HF	0.023	0.051	0.020	0.094

In addition, the properties at the BCPs can indicate the type of interaction present. The ρ_b values at the BCPs for complexes **1** – **4** in Table 1 are within the expected range for H-bonds, with only the ρ_b values of the Au^I···H interactions for **3.NH3** and **4.NH3** indicative of vdW-type interactions. The ρ_b values at the BCPs corresponding to the $(NH)_{carbene}$···X-H hydrogen bonds are higher than those of the Au···H interactions, indicating generally stronger H-bonds. The exceptions are those involving HF, where the ρ_b values for Au^I···H interaction in **1** and **2**

are 37 % higher than those of the NH···XH hydrogen bonds. The ρ_b values of the Au^{I}···H interaction for each Au complex decrease in the order HF > H_2O > NH_3 and simultaneously increase for the second H-bond in the order HF < H_2O < NH_3. These trends correlate with the NCI plots in shown Figure 2 and the bond lengths as previously discussed. In particular, the properties of the BCPs along the $(NH)_{carbene}$···X-H bonds are nearly identical for each XH, which corresponds to the very similar hydrogen-bond lengths seen in Figure 1. The small variations seen in Table 1 could be a result of the slight changes in N–H···X angle shown in Figure 1.

The $\nabla^2(\rho_b)$ values listed in Table 1 are all positive, characteristic of noncovalent interactions, and generally falling within the range expected for H-bonds as determined by Nakanishi *et al.* [55]. Furthermore, we note that the $\nabla^2(\rho_b)$ values of the $(NH)_{carbene}$···X hydrogen bonds involving H_2O and NH_3 are almost twice those of the Au···H hydrogen bond. It is surprising that the $\nabla^2(\rho_b)$ value for the Au^{I}···H interaction of the **3.H_2O** adduct is outside the range expected for H-bonds, since the ρ_b value falls within the H-bond range. However, it is only 0.003 $e a_0^{-5}$ less than what is expected for H-bonds, we thus describe this as a borderline case, i.e. a very weak H-bond with a substantial vdW contribution.

The Au···H interactions for the NH_3 hydrogen-bond donor are significantly weaker and characteristic of vdW-type interactions [55]. This may be due to the H atom being less acidic than H_2O and HF, or more likely that, since the NH···XH interaction is stronger for NH_3 (a stronger base) this forces the H atom to be further away from the Au, thus resulting in a weaker interaction. Nevertheless, the parameters at the BCPs are consistent with the geometrical parameters for the various Au···H hydrogen bonds; for instance, **1.NH_3**, **2.NH_3** and **3.H_2O** exhibit similar hydrogen bond distances and the parameters at the BCPs (Table 1) are practically identical. This indicates that Au···H hydrogen bonds display a relationship between bond length and BCP parameters. Since the BCPs of hydrogen-bonding interactions typically have ρ_b values greater than 0.01 according to Nakanishi *et al.*[55] Au···H hydrogen bonds can be identified based on the parameters of the BCPs shown in Table 1. Correlating this with the structures shown in Figure 1 suggests that Au···H hydrogen bonds typically are shorter than 2.79 Å.

Table 2 – Atomic charges (au) obtained using the Merz-Singh-Kollmann method at the MP2/aug-cc-pVTZ-pp level of theory.

		Δq(A) of the Au(I) centre in (*e*)		
	q(A) of Au(I)	**Δq**		
Complex	**monomer**	**NH_3**	**H_2O**	**HF**
1	-0.191	0.037	0.065	0.108
2	-0.166	0.042	0.085	0.080
3	0.047	0.031	0.040	0.060
4	0.149	-0.008	0.037	0.083

To gain further insight into the $Au^I\cdots H$ interaction, we also investigated the charges of the Au^I atom before adduct formation, obtained using the Merz-Singh-Kollmann method [56,57], as well as the change in the charge on the Au(I) centre upon adduct formation, see Table 2.

As expected, the electron-donating groups yield partial negative charges on the gold for **1** and **2**, while the electron-withdrawing groups induce partially positive charges on the Au(I) centre for **3** and **4**. Nevertheless, in all except one case (**4.NH_3)** the charge on the Au is less negative upon adduct formation. These results suggest that even if gold has a partial positive charge, it can still donate electron density and hence act as a Lewis base and H-bond acceptor. We noted similar behaviour for the $[(CF_3)_2Au]^-$ complex [2]. However, it has recently been argued by Clark and collaborators [58-60] that charge transfer is an unphysical construct, and effects such as those calculated here are better described by polarisation (these two terms are often grouped together as 'orbital effects'). Furthermore, they state that "Polarization and charge transfer are equivalent in the context of noncovalent interactions, and should be treated as such."[60] Since gold is known to be polarisable (for instance, it has been found that polarisation plays the dominant role in the bonding energy associated with adsorption involving Au [61]) the results shown in Table 2 could also be explained by variation in the polarisation of the Au(I) centres owing to the electron-donating or -withdrawing abilities of the R ligands.

Another general trend is that the change in charge is $\Delta q_{HF} > \Delta q_{H2O} > \Delta q_{NH3}$ for all complexes. This agrees with the Au⋯HX hydrogen bond lengths that suggest that the strength decreases in the order HF > H_2O > NH_3.

In a naive effort to establish the relative strengths of the various hydrogen bonding interactions a series of fixed scans were undertaken that systematically break the two hydrogen bonds, as shown in Scheme 1.

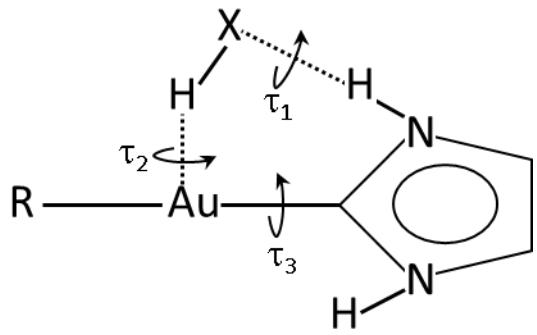

Scheme 1 – Definition of torsion angles systematically varied to break hydrogen bonds: Rotation around τ_1 and τ_2 break the NH···X hydrogen bond; rotation around τ_3 breaks Au···HX hydrogen bond.

Rotation of HF around τ_1 for the **2.HF** adduct (Figure 3(a)) results in the breaking of the Au···HF hydrogen bond, with a corresponding energetic penalty of 13.3 kcal/mol, while rotation around τ_2 breaking the $(NH)_{carbene}$···O hydrogen bond (Figure 3(b)) requires 6.1 kcal/mol at the B3LYP/aug-cc-pVTZ-pp level of theory. Since the total stabilisation for the **1.HF** adduct is –11.8 kcal/mol at this level of theory this suggests that breaking one hydrogen bond results in the almost complete simultaneous breakdown of the second hydrogen bond. This is, however, an artefact of the fixed scan undertaken since the hydrogen bond geometries in the adduct are not ideal in order to maximise both interactions. In order to accurately determine the effect of breaking one of the hydrogen bonds a relaxed scan should be undertaken, however all attempts failed to yield partially optimised geometries involving only one of the two hydrogen bonds. On the other hand, although rotation of H_2O around τ_3 for the **2.H_2O** adduct (Figure 4) involves breaking the NH···O hydrogen bond there is a low barrier suggesting that there is only a 4.1 kcal/mol energetic penalty. (The alternative NH···O hydrogen bond is 0.5 kcal/mol higher in energy as a result of a slight bending of the NHC ring towards the H_2O, with the two Au-C-N angles being 127.7° and 129.4°, respectively.) These results therefore suggest that hydrogen bond cooperativity may be present in the adduct, although the $(NH)_{carbene}$···X distances do not change with variation in R.

As described by Steiner in his review of hydrogen bonding [6], there are two types of cooperativity, namely σ-bond and π-bond cooperativity. σ-bond cooperativity, also described as "polarisation-assisted hydrogen bonding" involves the formation of a chain of hydrogen bonds, Y-H···X-H···A, where the presence of the Y-H···X hydrogen bond results in the X-H species becoming more polar and thus forming a stronger X-H···A hydrogen bond, and vice versa. This type of cooperativity could explain the non-linear orientations of the hydrides

relative to both the Au and the carbene NH groups in order to maximise both hydrogen bonds. However, the presence of σ-bond cooperativity would imply that the strength of the $(NH)_{carbene}\cdots X$ would change concomitantly with the Au···HX hydrogen bond upon varying the R group, which is not the case. It therefore seems unlikely that σ-bond cooperativity plays a role.

In π-bond cooperativity the hydrogen bonds stabilise a zwitterionic resonance form, such as O=C–N–H ↔ $^{-}$O–C=N^{+}–H [6]. The equivalent resonance forms for the complexes studied here are shown in Scheme 2, where the formation of the $(N–H)_{carbene}\cdots X$ hydrogen bond would mean that the first two resonance forms in Scheme 2 should dominate, particularly since Au is highly electronegative. The increase in negative charge on the Au^{I} centre would thus make it a better hydrogen-bond acceptor. Thus, it appears that π-bond cooperativity could play an important part in stabilisation upon hydrogen-bond formation with the HX species.

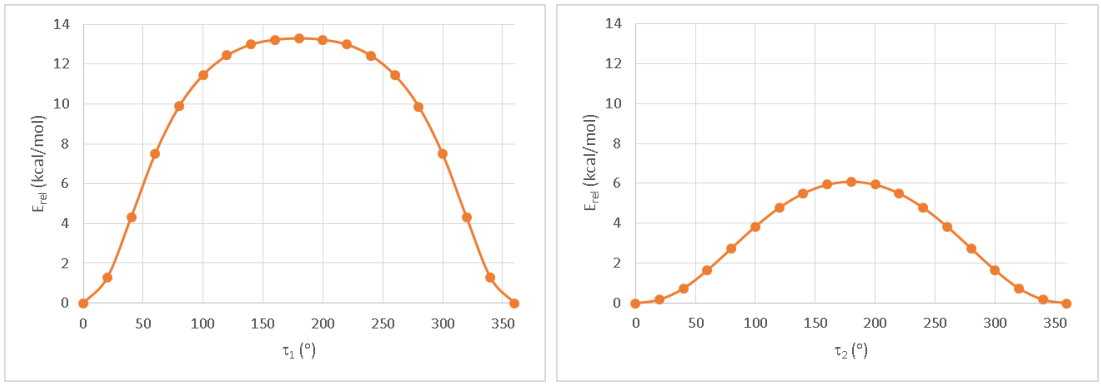

(a) (b)

Figure 3 – Change in relative energy (kcal/mol) with rotation around torsion angles (a) τ_1 and (b) τ_2 for **2.HF**.

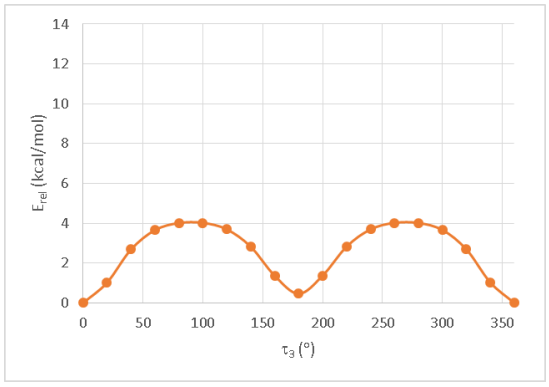

Figure 4 – Change in relative energy (kcal/mol) with rotation around torsion angle τ_3 for **2.HF**.

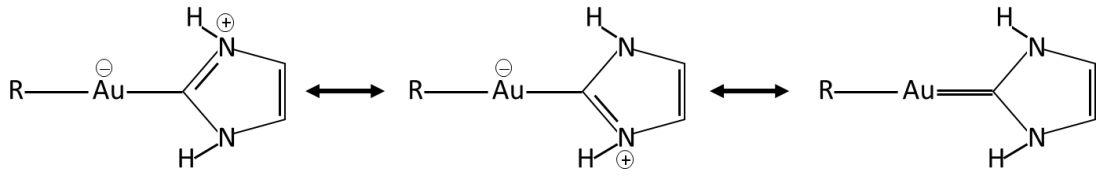

Scheme 2 – Proposed resonance forms involved in π-bond cooperativity.

NHC2 complexes

A second family of complexes with NHC2 = pyrrol-2-ylidene and R = H (**5**), CH_3 (**6**), Cl (**7**) and OH (**8**) interact with the hydrides in a similar way to the complexes with NHC1, also forming a second hydrogen bond to the NH group of the pyrrolylidene ring (Figure 5, Table S5 in ESI). In addition, in order to determine whether the $(NH)_{carbene}\cdots X$ hydrogen bonds are required to stabilise the adducts the conformational space was probed to identify if other minimum energy conformations where these hydrogen bonds were not present could be identified. By varying the starting geometries for the optimisations a second set of less stable adducts without $(NH)_{carbene}\cdots X$ hydrogen bonds was identified for each adduct (Figure 6, Table S6 in ESI).

All adducts of complexes **5** – **8** exhibit Au···HX hydrogen bonds, with those involving HF in general similar in distance and geometry to the Au···HF interactions obtained with complexes **1** – **4**. However, the Au···H distances to H_2O and NH_3 are marginally shorter and more linear than those involving complexes **1** – **4** suggesting that the interactions are stronger. The origin of this effect is probably the slightly greater electron-donating ability of the pyrrolylidene carbene relative to the imidazolylidene carbene. This is borne out by the marginally larger changes in the Merz-Singh-Kollman charges upon adduct formation (Table 3) than were observed for the NHC1 complexes (Table 2).

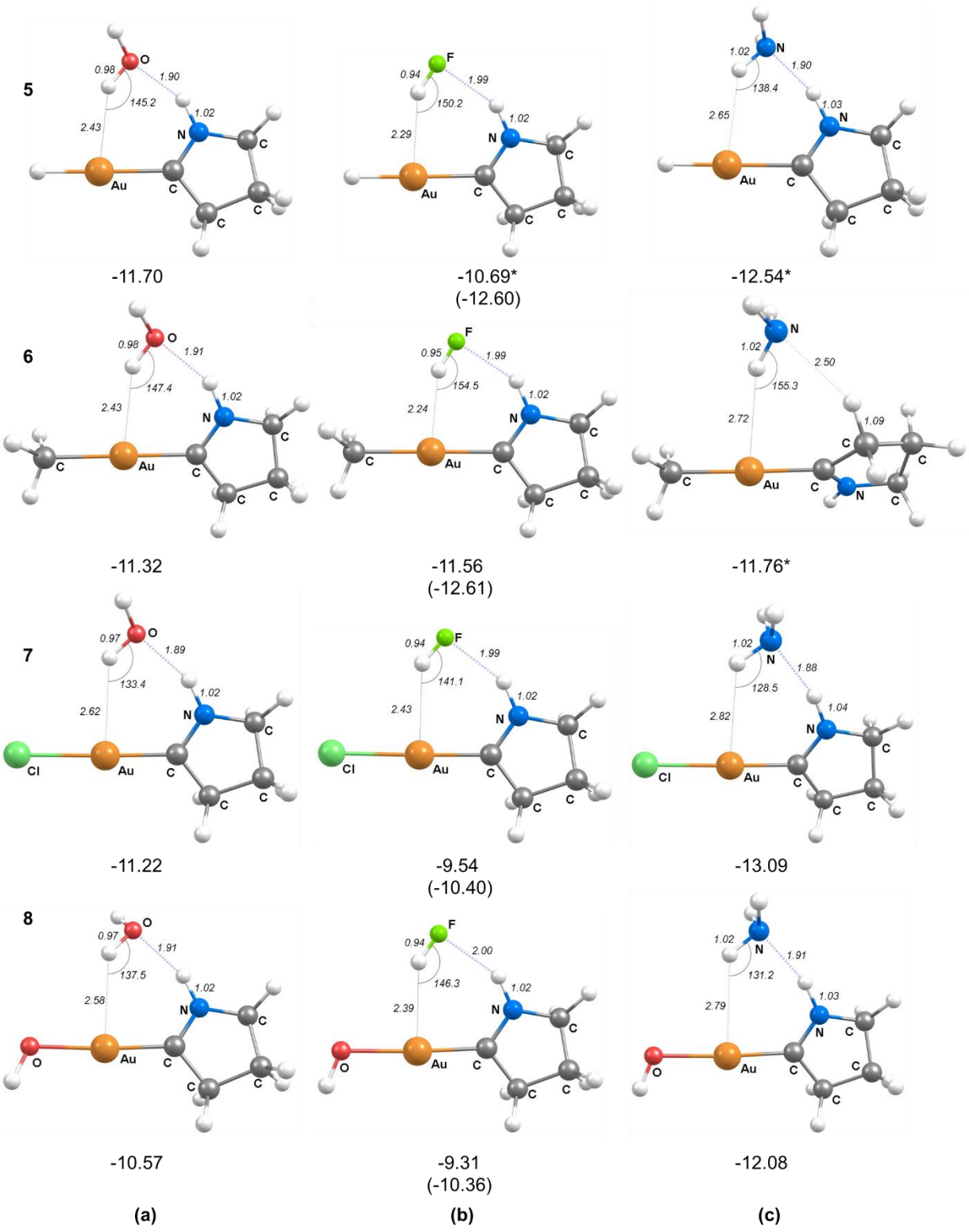

Figure 5 – Optimised geometries of complexes **5** – **8** H-bonded to (a) NH_3, (b) H_2O and (c) HF at the MP2/aug-cc-pVTZ-pp level of theory. Distances and angles are in Å and degrees, respectively. Counterpoise corrected values for the interaction energies in kcal/mol, E_{INT}, at the MP2/aug-cc-pVTZ-pp level of theory are given below each adduct (E_{INT} values at the B3LYP-D3/aug-cc-pVTZ-pp level of theory are given in parenthesis). *MP2/cc-pVTZ-pp value as MP2/aug-cc-pVTZ calculation did not complete owing to computational expense.

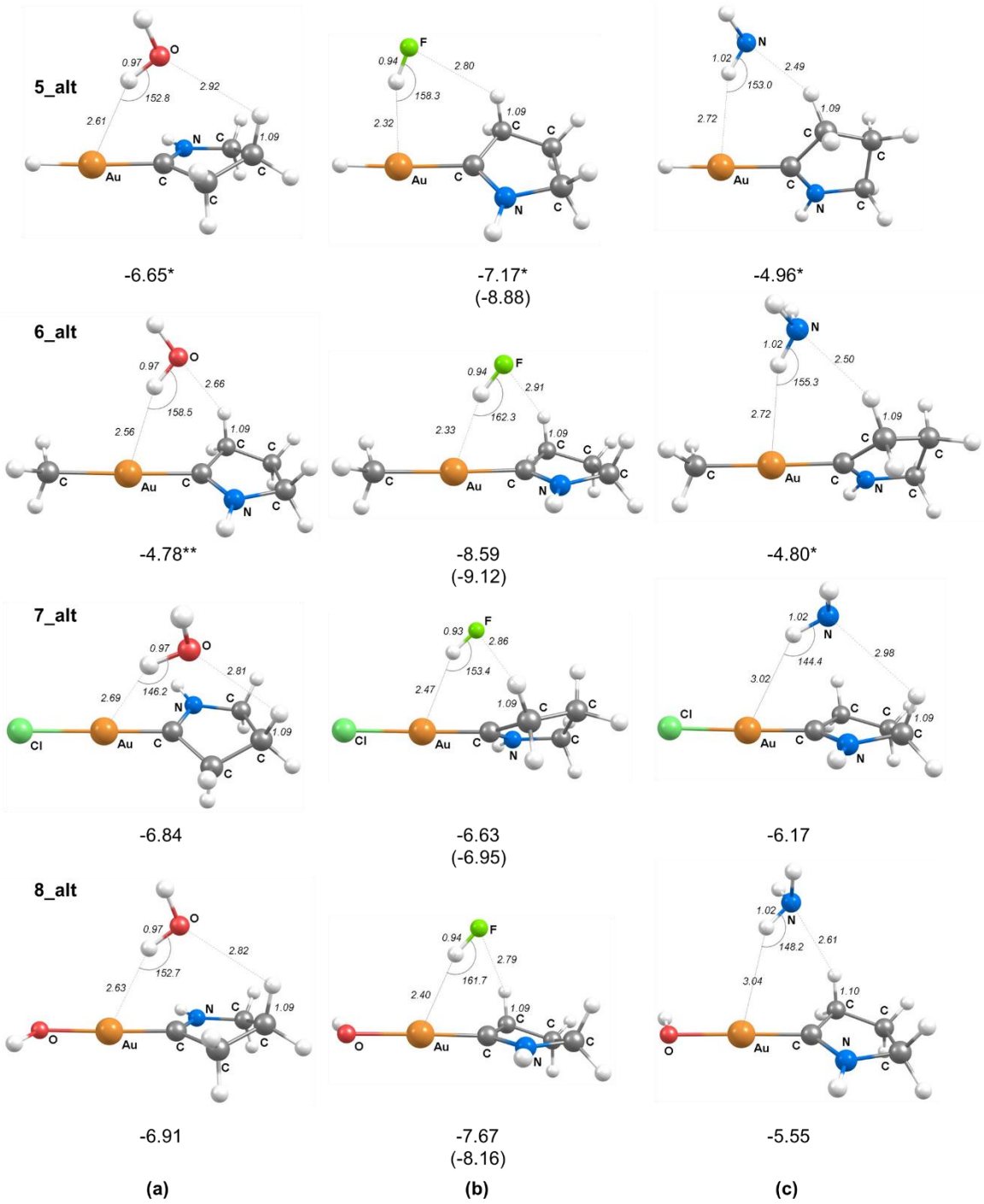

Figure 6 – Optimised geometries of complexes **5** – **8** H-bonded to (a) NH_3, (b) H_2O and (c) HF at the MP2/aug-cc-pVTZ-pp level of theory in alternative geometries that do not exhibit $(N\text{-}H)_{carbene}\cdots X$ hydrogen bonds. Distances and angles are in Å and degrees, respectively. Counterpoise corrected values for the interaction energies in kcal/mol, E_{INT}, at the MP2/aug-cc-pVTZ-pp level of theory are given below each adduct (E_{INT} values at the B3LYP-D3/aug-cc-pVTZ-pp level of theory are given in parenthesis). *B3LYP/aug-cc-pVTZ-pp value as the alternative geometry could not be found as a minimum on the MP2/aug-cc-pVTZ or MP2/cc-pVTZ-pp energy surfaces. **MP2/cc-pVTZ-pp value as MP2/aug-cc-pVTZ calculation did not complete owing to computational expense.

Table 3 – Atomic charges obtained using the Merz-Singh-Kollmann method at the MP2/aug-cc-pVTZ-pp level of theory.

		Δq(A) of the Au(I) centre in (*e*)		
	q(A) of Au(I)	**Δq**		
Complex	**monomer**	**NH_3**	**H_2O**	**HF**
5	-0.219	0.055	0.056	0.107
5_alt		0.022	0.022	0.067
6	-0.209	0.048	0.039	0.101
6_alt		0.008	0.013	0.094
7	0.027	0.026	0.019	0.030
7_alt		0.004	0.036	0.041
8	0.130	-0.004	-0.017	0.004
8_alt		0.030	0.089	0.092

In addition, the $(NH)_{carbene}\cdots X$ hydrogen bonds seen in Figure 5 are slightly weaker than those shown in Figure 1 (although again nearly identical for each hydride, independent of R), suggesting that the pyrrolylidene α-N–H unit is a weaker hydrogen bond donor than the imidazolylidene α-N–H. This could also result in less π-cooperativity than for complexes **1** – **4**, which could also contribute to the greater stabilisation in the adducts of **5** – **8**. Interestingly, the energies are quite similar for complexes **1** – **4** and **5** – **8**, suggesting that the decrease in $(NH)_{carbene}\cdots X$ hydrogen bond strength is balanced by the increase in Au···H–X strength.

In the alternative conformations of the adducts of **5** – **8** with the three hydrogen bond donors (Figure 6, Table S6 in ESI) the Au···H distances are similar (particularly for the HF adducts) or slightly longer than those found in adducts containing N-H···X interactions, further suggesting that hydrogen-bond cooperativity does indeed play a role in the formation of Au···HX hydrogen bonds. On the other hand, the hydrogen bond approach is more linear, as might be expected since the hydrogen bond donor no longer has to accommodate the formation of a second fairly strong hydrogen bond with the NH group.

Nevertheless, AIM analysis (Figure 7) shows that the deviation from linearity still present in **5** – **8** is the result of other, weaker CH···X interactions that exist. As seen from the properties of the BCPs along the Au···H-X and CH···X atomic interaction lines in Table 4, and visually on the NCI plots, the Au···H interactions now contribute more to the stabilisation than the

CH···X interactions. In fact, for the adducts with HF, the C-H···X interactions are so weak that no BCP is identified. Nevertheless, the NCI plots show a weak, very slightly attractive dispersion-type interactions between the fluorine on the HF and one of the CH units on the NHC2 ligand.

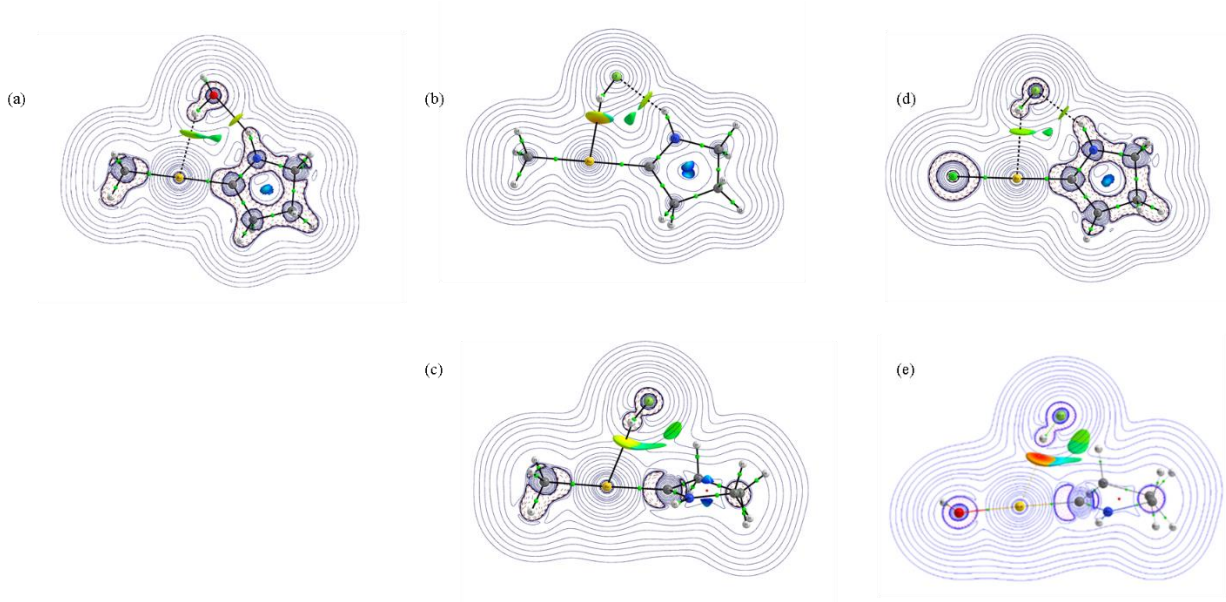

Figure 7 – The two-dimensional contour plot of $\nabla^2(\rho_b)$ (ea_0^{-5}) with the NCI plots shown as green to red areas on the images for selected adducts of complexes **5 - 8** with H_2O and HF: (a) **6.H$_2$O**, (b) **6.HF**, (c) **6.HF_alt**, (d) **7.HF**, (e) **8.HF_alt**. The red (minimum) regions indicate stabilising interactions, yellow/lime green regions indicate dispersion-type interactions and blue regions (maximum) coincide with repulsive intermolecular interactions.

Table 4 – Selected AIM parameters (au) for the BCPs of the indicated hydrogen bonds for the optimised structures of complexes **6** – **8** H-bonded to H_2O and HF at the MP2/aug-cc-pVTZ-pp level of theory.

	H-bond		Au···H-X		NH···X-H		CH···X-H	
			$\boldsymbol{\rho_b}$ $(\boldsymbol{ea_0^{-3}})$	$\boldsymbol{\nabla^2(\rho_b)}$ $(\boldsymbol{ea_0^{-5}})$	$\boldsymbol{\rho_b}$ $(\boldsymbol{ea_0^{-3}})$	$\boldsymbol{\nabla^2(\rho_b)}$ $(\boldsymbol{ea_0^{-5}})$	$\boldsymbol{\rho_b}$ $(\boldsymbol{ea_0^{-3}})$	$\boldsymbol{\nabla^2(\rho_b)}$ $(\boldsymbol{ea_0^{-5}})$
6	H_2O		0.021	0.047	0.028	0.094		
	HF	Au···H-X	0.030	0.049	0.020	0.084		
	HF_alt	Au···H-X	0.025	0.046			-	-
7	H_2O	Au···H-X	0.012	0.038	0.027	0.102		
	H_2O_alt	Au···H-X	0.011	0.035			0.005	0.020
	HF	Au···H-X	0.017	0.048	0.019	0.087		
	HF_alt	Au···H-X	0.019	0.042			-	-
8	H_2O	Au···H-X	0.013	0.040	0.026	0.099		
	H_2O_alt	Au···H-X	0.013	0.038			0.005	0.019
	HF	Au···H-X	0.019	0.049	0.019	0.049		
	HF_alt	Au···H-X	0.020	0.046			-	-

A change from the global minimum conformation with an $(NH)_{carbene}\cdots X$ hydrogen bond to the alternative conformations shown in Figure 6 could occur through simple rotation of the hydrogen bond donor around the linear R-Au-C axis as indicated in Scheme 3. The barrier to rotation of HF around the Au-C axis in **6.HF** (Scheme 2, Figure 6) is very low (<4.5 kcal/mol), suggesting that even the weak CH···X hydrogen bond found in the alternative conformation is sufficient to stabilise the adduct and that the HF is always involved in an interaction in addition to Au···H-X that varies in strength depending on the hydrogen bond donor on the NHC ring.

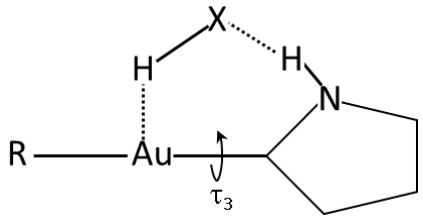

Scheme 3 – Rotation around τ_3 breaks NH···X hydrogen bond while maintaining Au···HX hydrogen bond.

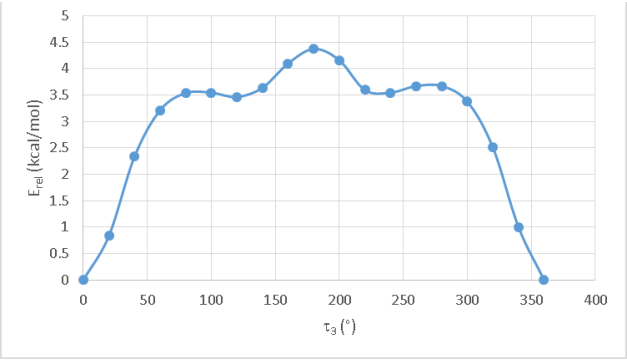

Figure 8 – Change in potential energy with rotation around τ_3 at the MP2/aug-cc-pVTZ-pp level of theory for **6.HF**.

NHC3 complex

Since it is clear from the results above that a second hydrogen bond contributes to the stabilisation of the Au···HX adduct, the importance of the presence of such an interaction for stabilising an Au···HX hydrogen bond was investigated. This was undertaken by further limiting the formation of $(NH)_{carbene}\cdots X$ hydrogen bonds through considering N-methyl substituted imidazolylidene ligands. In particular, CH···F interactions are known to be weak [62], and should therefore be less likely to form as second hydrogen bonds. Nevertheless, the interactions of the hydrogen bond donors with complex **9** containing NHC3 = 1,3-Me-imidazol-2-ylidene and R = CH_3 are similar to those found for the alternative conformations with the NHC2 complexes (Figure 9, Table S7 in the ESI). In all cases, the Au···HX hydrogen bonds occur with the now familiar variation in bond lengths. In addition, even though NH···X interactions are no longer possible, weaker CH···X interactions are still present, although these differ in the various adducts.

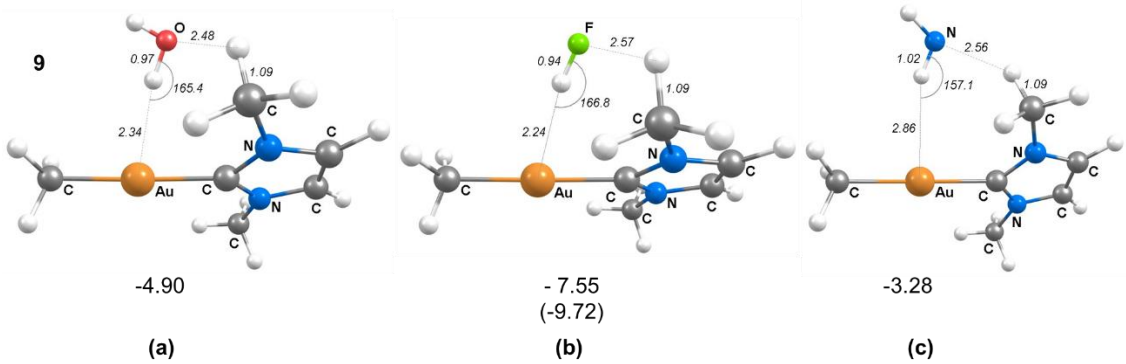

Figure 9 – Optimised geometries of complex **9** H-bonded to (a) NH_3, (b) H_2O and (c) HF at the MP2/aug-cc-pVTZ-pp level of theory. Distances and angles are in Å and degrees, respectively. Counterpoise corrected values for the interaction energies in kcal/mol, E_{INT}, at the B3LYP/aug-cc-pVTZ-pp level of theory are given below each adduct owing to computational expense of MP2/aug-cc-pVTZ-pp (E_{INT} value at the B3LYP-D3/aug-cc-pVTZ-pp level of theory is given in parenthesis).

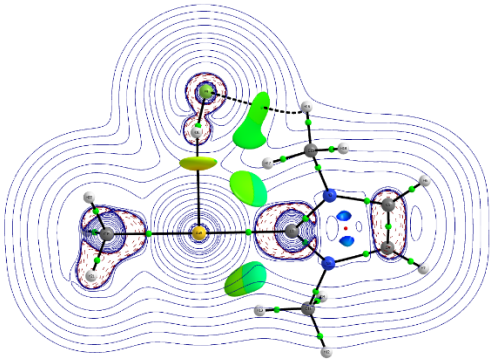

Figure 10 – The two-dimensional contour plot of $\nabla^2(\rho_b)$ (ea_0^{-5}) with the NCI plot shown as green to red areas on the images for complex **9** with HF. The red (minimum) regions indicate stabilising interactions, yellow/lime green regions indicate dispersion-type interactions.

AIM analysis (Figure 10, Table 5) confirms the presence of both the Au···HF hydrogen bond, which is similar in strength to those found previously based on the properties of the BCP, and a second H_2C-H···X interaction, which is considerably weaker than the Au···H interaction. According to the classification by Nakanishi [55] this Au···H interaction is a hydrogen bond, whereas the H_2C-H···X interaction is a van der Waals-type interaction. In addition, the NCI analysis suggests that there are further, even weaker but still attractive, dispersion interactions between C-H hydrogens and the Au(I) centre.

Table 5 – Selected AIM parameters for the optimised structures of complex **9** H-bonded to HF at the MP2/aug-cc-pVTZ-pp level of theory.

		H-bond	$\boldsymbol{\rho_b}$ $(\boldsymbol{e a_0^{-3}})$	$\boldsymbol{\nabla^2(\rho_b)}$ $(\boldsymbol{e a_0^{-5}})$
9	HF	Au···H-X	0.026	0.044
		CH···X-H	0.004	0.017

Merz-Singh-Kollmann charges (Table 6), suggest that there is more polarisation from the Au(I) centre to HF than to the other two H-bond donors.

Table 6 – Atomic charges obtained using the Merz-Singh-Kollmann method at the MP2/aug-cc-pVTZ-pp level of theory.

		Δq(A) of the Au(I) centre in (*e*)		
	q(A) of Au(I)	**Δq**		
Complex	**monomer**	**NH_3**	**H_2O**	**HF**
9	-0.106	0.006	0.009	0.059

Energy Decomposition Analysis

Although AIM and NCI yield complementary information about the strength and type of weak interactions they do not give any indication of the nature of the hydrogen bonds. Thus, to gain further insight, we undertook Energy Decomposition Analysis (EDA) of the adducts of **1** – **9** with HF (Figure 11 and Table S8 in the ESI) at the BP86-D3/TZP level of theory, with application of ZORA for describing the relativistic effects of gold, which we have shown previously is necessary for successfully describing hydrogen bonding [2, 3]. EDA supplements the AIM and NCI analyses by separating out the components of the interaction into electrostatic, Pauli repulsion, orbital and dispersion contributions, where the orbital interactions are described as being a combination of charge transfer and polarisation. For all

the adducts with the gold complexes the electrostatic and orbital contributions are similar in magnitude, with adduct formation for **1** – **8** involving ~50% electrostatics, 42% orbital interactions and <10% dispersion. For **9.HF**, 19% of the stabilisation found is from dispersion, confirming the results obtained with the NCI analysis (Figure 10).

Comparing the adducts of **5** – **8** in the conformations with and without the $(NH)_{carbene}\cdots X$ interactions enables us to establish the contribution made by these strong hydrogen bonds. For adducts of **5** – **8** in the alternative conformations, which do not exhibit the strong $(NH)_{carbene}\cdots X$ interactions, the electrostatic contribution is lower than when the $(NH)_{carbene}\cdots X$ hydrogen bonds are present (typically ~ 44% as compared to ~50%). There are also slightly larger contributions to orbital interactions and dispersion than for the conformations with $(NH)_{carbene}\cdots X$ hydrogen bonds (~43% and ~13% compared to 41% and ~9%, respectively). This suggests that the Au···H hydrogen bonds are less electrostatically driven than the $(NH)_{carbene}\cdots X$ hydrogen bonds, and instead involve more orbital interactions, most likely owing to the polarisability of the Au(I) centre, as we have suggested previously [63]. This also agrees with the changes observed in Merz-Singh-Kollmann charges (Tables 2, 4 and 6), which suggest that polarisation is important in stabilising the hydrogen-bonded adducts.

In a further effort to confirm the contribution of the $(NH)_{carbene}\cdots X$ hydrogen bonds to the overall stabilisation, EDA analysis of the adducts of HF with the carbenes NHC1 and NHC3 without the Au(I) and the second ligand, but in the same geometries as adducts **1.HF** and **9.HF**, respectively, was performed (Figure 12). The differences between the components of **1.HF** and **9.HF** and **NHC1.HF** and **NHC3.HF** are also shown in Figure 12 as a rough estimate of the components of the Au···HF hydrogen bonds. The EDA analysis shows that since the formation of the **NHC1.HF** and **NHC3.HF** adducts is indeed primarily electrostatically driven (>60% contribution of electrostatics to the attractive interactions), as would be expected for moderate N-H···F hydrogen bonds, the Au···HF hydrogen bond involves a relatively greater orbital interaction.

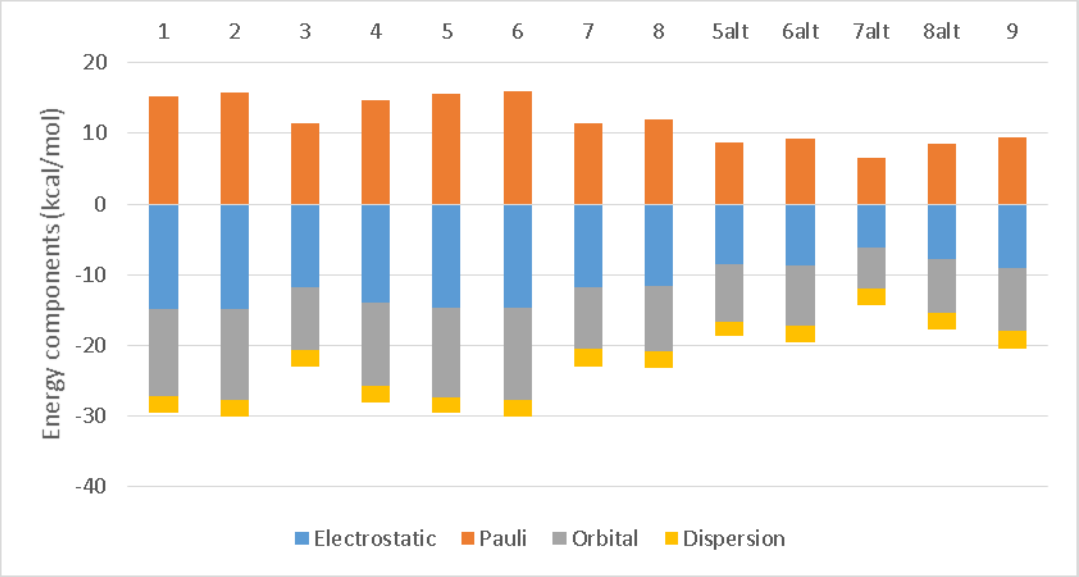

Figure 11 – Components of interactions between complexes **1 – 9** and HF at the BP86-D3/TZVP level of theory.

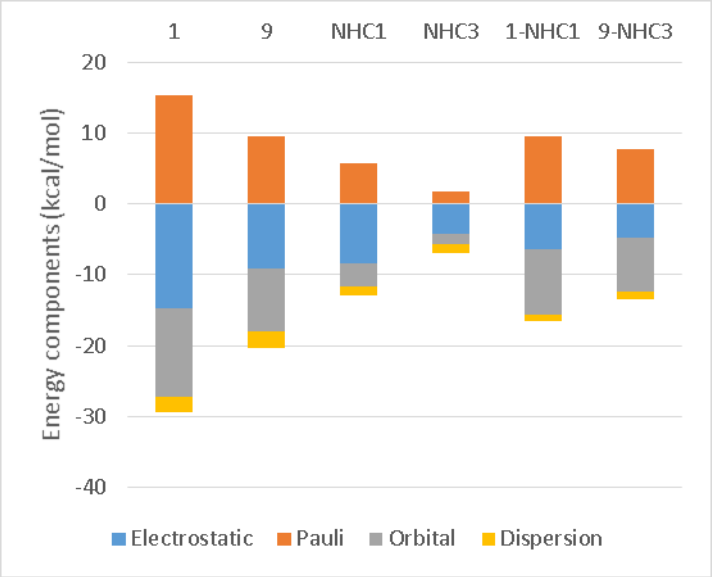

Figure 12 – Components of interactions involving NHC1 and NHC3 with HF at the BP86-D3/TZVP level of theory.

Summary

High quality wave functions of adducts of the neutral Au(I) complexes **1** – **9** with NH_3, H_2O and HF analysed using AIM and NCI confirm that these form Au···H hydrogen bonds since they exhibit BCPs along the atomic interaction lines connecting the Au and H that correspond to attractive interactions. The highest accumulation of electron density between the Au and H atoms occurs when R = CH_3 and the lowest when R = Cl for all the H-bond donors and NHCs. This trend follows the resultant Lewis basicity of the Au(I) centre within the complexes and agrees with the calculated atomic charges, where it was found that the hydride and methanide

analogues produced the largest partial negative charges on the Au(I) atom. In addition, the change in charge follows the same trends, suggesting that the Au···H interaction is not only electrostatic in origin, but that polarisation also plays a role. This was confirmed by EDA analysis, where the orbital term, *i.e.* polarisation, was shown to play the most important role in the Au···H hydrogen bond, in contrast with the $(NH)_{carbene}$···X hydrogen bonds, which are primarily electrostatically driven. This is probably due to the greater polarisability of Au relative to the X hydrogen bond acceptors.

Furthermore, the AIM and NCI results suggest that for the Au···H interaction to occur in complexes containing the NHC1 ligand (complexes **1** – **4**), a second H-bond, i.e. the $(NH)_{carbene}$···XH interaction, must be present to aid in stabilising the adducts. In effect, the involvement of the amphiprotic main group hydrides in two interactions results in the formation of a pseudo chelate with κ^2-C-H coordination. In all adducts of NH_3, H_2O and HF and complexes **5** – **8** containing the NHC2 ligand (with only one α-N–H unit that can form an $(NH)_{carbene}$···X hydrogen bond) and complex **9** (with the NHC3 ligand with no N–H units) a second interaction in addition to the Au···H hydrogen bond was found to be present; this was usually a weak C-H···X interaction, but AIM analysis showed that sometimes even weak dispersion-type interactions could be identified. Scans of the potential energy surface suggest that π-cooperativity plays a role in stabilising these adducts.

The overall stability of the adduct results from a compromise between satisfying the geometrical requirements of the two hydrogen bonds, thus leading to large deviations from linearity. For instance, **3**.**NH$_3$** has the highest E_{INT} despite having the weakest Au···H interaction based on the AIM parameters. For H_2O and NH_3 the $(NH)_{carbene}$···XH interactions add the most stabilisation to the total E_{INT} values and are generally independent of the R groups, whereas Au···H interactions dominate the stabilisation of all adducts involving HF, and are strengthened by the presence of electron-donating R groups.

In conclusion, the results presented here are able to address the questions raised by Kazarian *et al*. [1] and Schmidbaur *et al*. [2] and confirm that intermolecular hydrogen bonds involving neutral Au(I) complexes can theoretically exist. Furthermore, we have shown that the presence of a second hydrogen bond gives additional stabilisation to the adduct. Therefore, a strategy for designing neutral gold complexes that can form Au···HX hydrogen bonds would be the inclusion of a strong hydrogen-bond donor in a suitable orientation to allow the simultaneous formation of a pseudo chelate by involving both Au···HX and $(NH)_{carbene}$···XH hydrogen bonds.

References

1. Kazarian SG, Hamley PA, Poliakoff M (1993) J Am Chem Soc 115: 9069-9079.
2. Groenewald F, Dillen J, Raubenheimer HG, Esterhuysen C (2016) Angew Chem Int Ed 55: 1694-1698.
3. Groenewald F, Dillen J, Raubenheimer HG, Esterhuysen C (2017) Dalton Trans 46: 4960-4967.
4. Schmidbaur H, Raubenheimer HG, Dobrzañska L (2014) Chem Soc Rev 43: 345-380.
5. Koskinen L, Jääskeläinen S, Kalenius E, Hirva P, Haukka M (2014) Cryst Growth Des 14: 1989-1997.
6. Steiner T (2002) Angew Chem Int Ed 41: 48-76.
7. Kryachko ES (2008) J Mol Struct 880: 23-30.
8. Brammer L, Zhao D, Ladipo FT, Braddock-Wilking J (1995) Acta Crystallog B51: 632-640.
9. Groom CR, Bruno IJ, Lightfoot MP, Ward SC (2016) Acta Crystallog B72: 171-179.
10. Collado A, Gomez-Suarez A, Martin AR, Slawin AMZ, Nolan SP (2013) Chem Commun 49: 5541-5543.
11. Phillips N, Dodson T, Tirfoin R, Bates JI, Aldridge S (2014) Chem Eur J 20: 16721-16731.
12. Nahra F, Patrick SR, Collado A, Nolan SP (2014) Polyhedron 84: 59-62.
13. Kunz PC, Wetzel C, Kögel S, Kassack MU, Spingler B (2011) Dalton Trans 40: 35-37.
14. Raubenheimer HG, Lindeque L, Cronje S (1996) J Organomet Chem 511: 177–184.
15. Jeffrey GA (1997) An Introduction to Hydrogen Bonding. Oxford University Press, Oxford.
16. Groenewald F, Esterhuysen C, Dillen J (2012) Theo Chem Acc 131: 1-12.
17. Riley KE, Hobza P (2007) J Phys Chem A 111: 8257-8263.
18. Boys SF, Bernardi F (1970) Mol Phys 19: 553-566.
19. Simon S, Duran M, Dannenberg JJ (1996) J Chem Phys 105: 11024-11031.
20. Frisch MJ, Trucks GW, Schlegel HB, Scuseria GE, Robb MA, Cheeseman JR, Scalmani G, Barone V, Mennucci B, Petersson GA, Nakatsuji H, Caricato M, Li X, Hratchian HP, Izmaylov AF, Bloino J, Zheng G, Sonnenberg JL, Hada M, Ehara M, Toyota K, Fukuda R, Hasegawa J, Ishida M, Nakajima T, Honda Y, Kitao O, Nakai H, Vreven T, Montgomery JA, Peralta JE, Ogliaro F, Bearpark M, Heyd JJ, Brothers E, Kudin KN, Staroverov VN, Kobayashi R, Normand J, Raghavachari K, Rendell A,

Burant JC, Iyengar SS, Tomasi J, Cossi M, Rega N, Millam JM, Klene M, Knox JE, Cross JB, Bakken V, Adamo C, Jaramillo J, Gomperts R, Stratmann RE, Yazyev O, Austin AJ, Cammi R, Pomelli C, Ochterski JW, Martin RL, Morokuma K, Zakrzewski VG, Voth GA, Salvador P, Dannenberg JJ, Dapprich S, Daniels, AD, Farkas, Foresman JB, Ortiz JV, Cioslowski J, Fox DJ (2009) Gaussian 09, Revision B.01.

21. Becke AD (1998) J Chem Phys1993. 98: 5648-5652.
22. Lee C, Yang W, Parr RG (1988) Phys Rev B 37: 785-789.
23. Miehlich B, Savin A, Stoll H, Preuss H (1989) Chem Phys Lett, 1989. 157: 200-206.
24. Tao J, Perdew JP, Staroverov VN, Scuseria GE (2003) Phys Rev Lett, 2003. 91: 146401.
25. Peterson KA, Puzzarini C (2005) Theo Chem Acc 114(4-5): 283-296.
26. Figgen D, Rauhut G, Dolg M, Stoll H (2005) Chem Phys 311: 227-244.
27. Kendall RA, Dunning TH, Harrison RJ (1992) J Chem Phys 96: 6796-6806.
28. Dunning TH (1989) J Chem Phys 90: 1007-1023.
29. Møller C, Plesset MS (1934) Phys Rev 46: 618-622.
30. Binkley JS, Pople JA (1975) Int J Quant Chem 9: 229-236.
31. Feller D (1996) J Comp Chem 17: 1571-1586.
32. Schuchardt KL, Didier BT, Elsethagen T, Sun L, Gurumoorthi V, Chase J, Li J, Windus TL (2007) J Chem Inf Model 47: 1045-1052.
33. Zhurko GA, Zhurko DA (2012) ChemCraft.
34. Bondi A (1964) J Phys Chem 68: 441-451.
35. Keith TA (2012) AIMAll version 14.06.21. TK Gristmill Software.
36. Keith TA, Frisch MJ, J Phys Chem A115: 12879-12894.
37. Tiana D, Francisco E, Blanco MA, Martin Pendás A (2009) J Phys Chem A 113: 7963-7971.
38. Johnson ER, Keinan S, Mori-Sánchez P, Contreras-García J, Cohen AJ, Yang W (2010) J Am Chem Soc 132: 6498-6506.
39. Bickelhaupt FM, Baerends EJ (2000) In: Lipkowitz KB, Boyd DB (eds) Rev. Comput. Chem. Vol. 15 Wiley-VCH, New York, pp 1–86.
40. Morokuma K (1971) J Chem Phys 55: 1236.
41. Ziegler T, Rauk A (1977) Theor Chim Acta 46: 1-10.
42. Te Velde G, Bickelhaupt FM, Baerends EJ, Fonseca Guerra C, van Gisbergen SJA, Snijders JG, Ziegler T (2001) J Comput Chem 22: 931-967.

43. a) Becke AD (1988) Phys Rev A 38: 3098-3100; b) Perdew JP (1986) Phys Rev B 33: 8822-8824.
44. a) van Lenthe E, Baerends EJ, Snijders JG (1994) J Chem Phys 101: 9783; b) van Lenthe E, Ehlers A, Baerends EJ (1999) J Chem Phys 110: 8943.
45. Grimme S, Antony J, Ehrlich S, Krieg H (2010) J Chem Phys 132: 154104.
46. Etter MC, MacDonald JC, Bernstein J (1990) Acta Crystallog B 46: 256-262.
47. Grabowski SJ (2004) J Phys Org Chem 17: 18-31.
48. Berger RJF, Schoiber J, Monkowius U (2017) Inorg Chem 56: 956-961.
49. Rigoulet M, Massou S, Sosa Carrizo ED, Mallet-Ladeira S, Amgoune A, Miqueu K, Bourissou D (2019) Proc Natl Acad Sc. USA 116: 46-51.
50. Cukrowski I, de Lange JH, Groenewald F, Raubenheimer HG (2017) ChemPhysChem 18: 2288-2294.
51. Grabowski SJ (2001) J Phys Chem A105: 10739-10746.
52. González L, Mó O, Yáñez M, Elguero J (1998) J Chem Phys 109: 2685-2693.
53. Koch W, Frenking G, Gauss J, Cremer D, Collins JR (1987) J Am Chem Soc 109: 5917-5934.
54. Rozas I, Alkorta I, Elguero J (2000) J Am Chem Soc 122: 11154-11161.
55. Nakanishi W, Hayashi S, Narahara K (2008) J Phys Chem A112: 13593-13599.
56. Singh UC, Kollman PA (1984) J Comp Chem 5: 129-45.
57. Besler BH, Merz KM Jr., Kollman PA(1990) J Comp Chem 11: 431-39.
58. Clark T (2017) Faraday Discuss 203: 9-27.
59. Clark T (2017) J Mol Model 23: 297.
60. Clark T, Murray JS, Politzer P (2018) Phys Chem Chem Phys 20: 30076-30082.
61. Hernández NC, Graciani J, Márquez A, Sanz JF (2005) Surf Sci 575: 189-196.
62. Desiraju GR, Steiner T (1999) The Weak Hydrogen Bond in Structural Chemistry and Biology. In: IUCr Monographs on Crystallography, Vol. 9. Oxford University Press, New York.
63. Groenewald F, Dillen J, Esterhuysen C (2018) New J Chem 42: 10529-10538.